Received 13 October 2022; revised 8 December 2022; accepted 24 December 2022. Date of publication 5 January 2023;
date of current version 23 January 2023.

Digital Object Identifier 10.1109/OJAP.2023.3234341

New Self-Isolated Wideband MIMO Antenna System for 5G mm-Wave Applications Using Slot Characteristics

OLUDAYO SOKUNBI[1] (Graduate Student Member, IEEE), HUSSEIN ATTIA[2,3] (Member, IEEE), ABUBAKAR HAMZA[2,3] (Student Member, IEEE), ATIF SHAMIM[4] (Senior Member, IEEE), YIYANG YU[4] (Graduate Student Member, IEEE), AND AHMED A. KISHK[1] (Life Fellow, IEEE)

[1]Electrical and Computer Engineering Department, Concordia University, Montreal, QC H3G 1M8, Canada

[2]Center for Communication Systems and Sensing, King Fahd University of Petroleum and Minerals, Dhahran 31261, Saudi Arabia

[3]Electrical Engineering Department, King Fahd University of Petroleum and Minerals, Dhahran 31261, Saudi Arabia

[4]Computer, Electrical, Mathematical Science and Engineering Division, King Abdullah University of Science and Technology, Thuwal 23955, Saudi Arabia

CORRESPONDING AUTHOR: H. ATTIA (e-mail: hattia@kfupm.edu.sa)

This work was supported by the King Fahd University of Petroleum and Minerals (KFUPM). The work of Hussein Attia and Abubakar Hamza was supported by the Interdisciplinary Research Center for Communication Systems and Sensing under Grant INCS2106.

ABSTRACT This paper proposes a simple novel technique for self-isolating a MIMO antenna for mm-wave applications. MIMO antenna elements with inter-element separation of 0.2 mm (0.023λ at 35 GHz) and measured high isolation ($>$ 50 dB) are presented. By observing the concentration of surface waves on the radiating patch, several rigorously optimized slots of different shapes, positions, and dimensions are etched on the patch to enhance the inter-element isolation and increase the bandwidth within 28-37.5 GHz. The circuit models of the reference and proposed antennas have been presented. The coupling is measured by the level of the differences in the output voltage in both antennas. The novel mm-wave antenna exhibits high impedance bandwidth ($>$ 29%), high isolation ($>$ 50 dB), high efficiency ($>$ 90%), and low envelope correlation coefficient ($<$0.005). Two configurations of MIMO antenna (i.e., 1×2 and 1×4) are fabricated and measured to validate the simulation outcomes. The single reference antenna has dimensions of 10x12 mm^2 while the 1x2 array has dimensions of 19x12 mm^2. The presented design is the first to exhibit such wideband isolation improvement without any external decoupling structure at the mm-wave frequency range, to the best of the authors' knowledge.

INDEX TERMS Self-isolated antenna, mm-waves, multiple-input-multiple-output (MIMO), 5G antennas, patch antenna, surface waves, mutual coupling.

I. INTRODUCTION

THE 5G wireless technology offers high data rate, low latency, low energy and cost, increased spectral efficiency and channel capacity, especially when used in MIMO technology [1], [2]. Therefore, mm-wave antenna arrays are explored to meet the user requirements of high throughput, with a very close distance between antenna elements to enable miniaturization [3]. However, antenna arrays design at mm-wave bands has been a growing concern among antenna engineers because of the inevitable, undesired mutual coupling between the antenna elements [4].

Various techniques have been reported in the literature to mitigate mutual coupling at mm-wave bands [5], [6], [7], [8], [9], [10], [11], [12], [13], [14], [15], [16], [17], [18], [19], [20]. The defective fractal ground was reported by [5] to achieve 13 dB isolation improvement between two compact patch antenna arrays in the 11.4-11.78 GHz range. Metasurfaces have been used to achieve a maximum of 15 dB isolation improvement within 27-32 GHz [6]. A maximum of 31.5 dB mutual coupling reduction at 60.4 GHz was achieved in [7] using a metasurface shield. The authors in [8] proposed Complementary Split Ring Resonator (CSRR) as

a decoupling element in a MIMO array to achieve 31.8 dB isolation improvement and improved the radiation characteristics within 24.7-25.3 GHz. Defected Ground Surfaces (DGS) [9] were used to enhance the isolation of two integrated antenna systems by 3 dB in the dual-band of 4G (3.8 and 5.5 GHz), and 5 dB in the 5G bands (24.4-29.3 GHz). Frequency Selective Surface (FSS) was reported to increase the isolation of a dielectric resonator (DRA) MIMO antenna by a maximum of 30 dB in the 57-63 GHz bandwidth [10]. In [11], a hybrid isolator was used as an EBG unit cell to improve the isolation of a MIMO dielectric resonator antenna by a maximum of 25 dB within 59.3-64.8 GHz impedance bandwidth. The authors in [12] have used metallic vias as a decoupling mechanism to achieve about 19.8 dB isolation improvement in the E-plane, and 22.7 dB in the H-plane of a 1 × 2 MIMO DRA antenna at 26 GHz. Metal strips were printed on a MIMO DRA to achieve a maximum isolation improvement of 12 dB at 27.5-28.35 GHz [13]. The authors in [15] used multiple notches structures on the ground planes of a MIMO Vivaldi antenna to achieve a 37.3 dB maximum mutual coupling reduction enhancement within 24.55-28.5 GHz. The feed line structure of a 56.5-64 GHz slot patch antenna was modified to achieve a maximum isolation improvement of 38.6 dB [16]. Several Electromagnetic Band Gap (EBG) surfaces were employed as decoupling structures in [17], [18], [19]. Defective Ground Surface (DGS) was used by [20] to decouple a slot-array patch antenna by 50 dB between 1.2-1.35 GHz. In [21], the authors used near-field resonator placed above 2 and 8-element patch antennas to realize a 20 dB coupling reduction within 6.1% bandwidth. Also, the authors in [22] proposed the use of the dielectric block to achieve over 20 dB coupling reduction between very close patch antenna elements in both E- and H-planes around 4.32-5.48 GHz bandwidth.

Recently, antenna engineers have been considering inherently isolated MIMO antennas that do not require additional isolating structures. These antennas are more compact with reduced complexity and cost [23], [24], [25], [26], [27], [28], [29], [30], [31]. Some researchers have discussed self-isolated antennas. In [23], a slot rotated at 45° was utilized between a substrate-integrated waveguide with two-edged shorted vias to achieve maximum isolation, efficiency, and ECC of 18.5 dB, 79.2% and 0.02, respectively, at 3.45-3.55 GHz. Li et al. [24] proposed an eight open-slot MIMO antenna array for smartphones over 3.4-3.6 GHz with more than 17.5 dB isolation. Moreover, a MIMO patch antenna for mobile phones with mutual coupling less than 17 dB over 3.4-3.6 GHz was reported [25].

This paper presents a simple, yet efficient, self-isolated MIMO antenna system in the 5G mm-wave frequency band. Tightly spaced patch antenna MIMO elements with a maximum isolation *enhancement* of 35 dB over the 28-37.5 GHz mm-wave frequency band is achieved. The impedance bandwidth and isolation improvements are enabled by meticulously introducing U-slot, H-slot, and five circular slots on the patch, which are illustrated by studying the surface current distributions. The authors believe that this is the first time such concept is reported at the mm-wave frequency band of 28 GHz. 1 × 2 and 1 × 4 MIMO antenna arrays are presented to validate the proposed novel isolation mechanism. The proposed antenna exhibits high gain, efficiency, low correlation coefficient, and good radiation properties throughout the working bandwidth. The proposed highly isolated antenna is fabricated and tested.

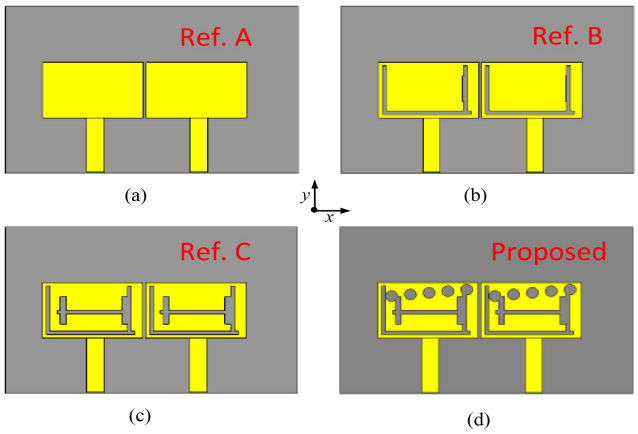

FIGURE 1. Design evolution of the proposed 1 × 2 MIMO antenna: (a) No slots (Ref. A) (b) Ref. A with U-slot (Ref. B) (c) Ref. B with H-slot (Ref. C) (d) Ref. C with five circular slots (proposed design).

The manuscript is organized as follows: Section II describes the antenna structure, which includes the evolution (i.e., development stages) of the proposed antenna array, the concept of wideband self-isolation, and the parametric analyses. Section III illustrates a 4-element antenna array to verify the MIMO capability of the proposed antenna, while Section IV concludes the paper.

II. ANTENNA STRUCTURE AND DEVELOPMENT

In this Section, first, the design methodology of the MIMO antenna is discussed. The self-isolation mechanism is then thoroughly explained through the equivalent circuit models and S-parameter results. Rigorous parametric analyses are also presented to optimize the performance of the MIMO antenna. Finally, far-field results are presented and discussed.

A. ANTENNA DESIGN AND EVOLUTION

Figure 1 demonstrates the evolution of the proposed antenna from a simple reference antenna (Ref. A) to the proposed antenna. Each antenna in Fig. 1 consists of two copper patches, each with 0.035 mm thickness, mounted on Rogers RT5870 substrate of dielectric constant 2.33, loss tangent 0.0012, height 0.508 mm, and a total size of 19x12 mm^2. The patch dimensions are accurately designed to operate at the mm-wave frequency band of 28 GHz. The two antennas are placed side-by-side along the x-axis (H-plane) with an edge-to-edge distance of 0.2 mm. The two patches are fed

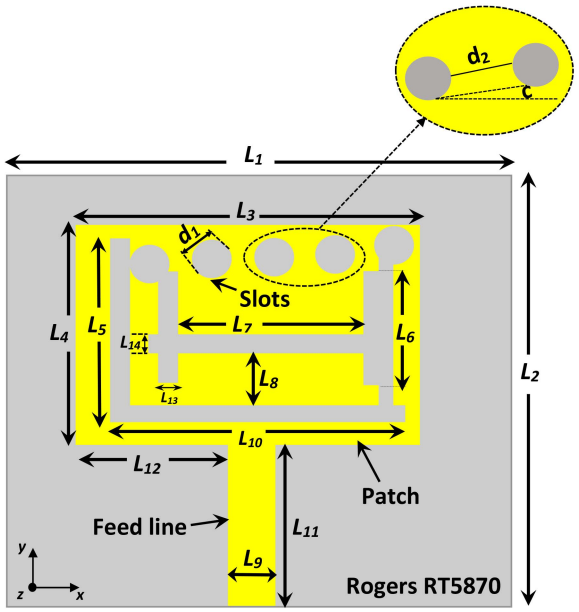

FIGURE 2. Geometry of the proposed self-isolated 5G mm-wave antenna.

TABLE 1. Dimensions of the self-isolated MIMO antenna.

Parameters	L_1	L_2	L_3	L_4	L_5	L_6	L_7	L_8
Values (mm)	10	12	6.5	4	3.5	2.0	3.64	1.24
Parameters	L_9	L_{10}	L_{11}	L_{12}	L_{13}	L_{14}	d_1	d_2
Values (mm)	1.11	5.75	3.9	2.86	0.36	0.25	0.78	0.45

with 50 Ω microstrip lines, each line with optimized dimensions of 1.11 mm x 3.9 mm and located at $L_{12} = 2.86$ mm (See Fig. 2).

From Fig. 1, to realize the proposed antenna with a wide bandwidth and improved isolation between the elements, a design evolution is performed where the initial reference antenna is denoted as Ref. A. Then, a U-slot is etched on Ref. A antenna to form Ref. B antenna. Another H-slot is etched on Ref. B antenna to form Ref. C antenna. Finally, five circular slots are etched on the Ref. C antenna to realize the proposed structure.

The circular slots have a diameter $d_1 = 0.78$ mm, while the rectangular slots have a thickness $L_{14} = 0.25$ mm. The five circular slots are separated from each other by $d_2 = 0.45$ mm and tilted by an angle of $c = 5.4°$. The effect of the different slot shapes on the antenna's bandwidth improvement and isolation enhancement is thoroughly explained in the subsequent sections. Fig. 2 shows the optimized structure and dimensions of the proposed antenna. Table 1 shows the dimensions of the proposed antenna. It is worthy of note that the U, H, and circular slots were used as a result of meticulous observation of the surface currents on the patch and the effect of different types of slots on the antenna coupling. As a result, the considered slots' shapes exhibit better coupling reduction compared to others due to further surface current reduction.

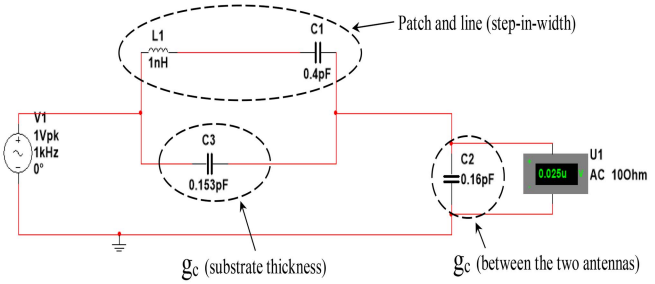

FIGURE 3. Equivalent circuit model of the reference antenna (Ref. A) simulated using NI Multism software.

B. EQUIVALENT CIRCUIT AND DECOUPLING CONFIGURATION

The equivalent circuit of the reference antenna (Ref. A) is a modified version of the equivalent circuit of an inset-fed microstrip antenna [31], [32]. As seen in Fig. 3, the feedline and patch are represented by series step-in-width L-C elements, connected in parallel with a gap capacitor of capacitance (g_c), caused by the ground and the radiating patch. This combination is connected in series to another gap capacitor of capacitance (g_c), caused by the separation between the two antennas. The inductance (L) and capacitance values (C) of the step-in-width feedline and patch are calculated using the step-in-width formulas [32]:

$$L = \frac{I_L Z_{OL}}{f\lambda_g} \tag{1}$$

$$C = \frac{I_L}{Z_{OL} f \lambda_g} \tag{2}$$

While the gap capacitance (g_c) is calculated as follows [33]:

$$g_c = \frac{2.531}{g^{0.782}} \quad [pF/mm] \tag{3}$$

where I_L is the element length (in mm), Z_{OL} is the element impedance assumed to be 50 Ω, f is the central operating frequency taken as 35 GHz and λ_g is the guide wavelength. Equations (1) and (2) are used to derive the values of L_1 and C_1 seen in Fig. 3, while (3) is used to derive C_2 and C_3. The parameter g used in (3) is the distance measured in μm between the two antennas (for C_2) and the thickness of the substrate (for C_3). The element lengths I_L of the patch and feedline are equal to L_4, and L_{11}, respectively, as shown in Fig. 2. From Fig. 3, L_1 and C_1 are the equivalent inductance and capacitance of the patch and feedline. The coupling between the two antennas is assumed to be capacitive due to the electric field between both antennas. Using National Instruments (NI) Multisim software, an AC voltage source of 1 V peak is used to excite the circuit in Fig. 3. A voltage 25 nV is obtained as the coupling voltage transferred to the other antenna, measured across C_2.

Using the same concept, the equivalent circuit model of the proposed self isolated MIMO antenna is developed and depicted in Fig. 4. C_1- C_{15} are derived using Equation (3),

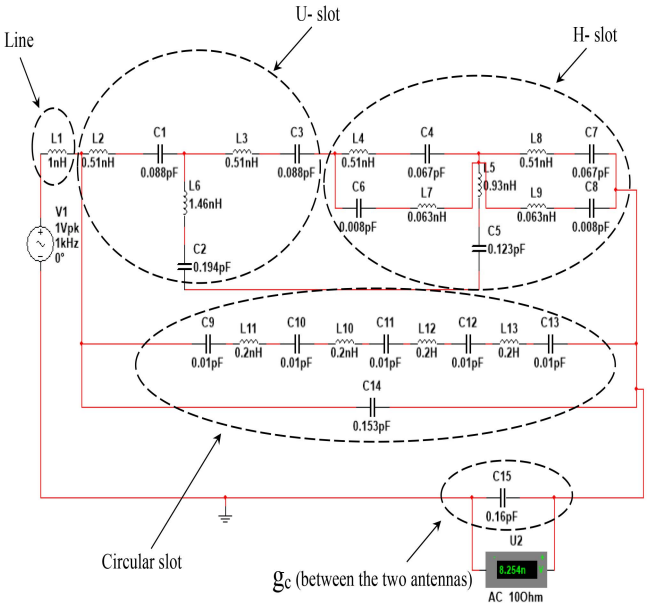

FIGURE 4. Equivalent circuit model of the proposed 5G mm-wave antenna with several slots simulated using NI Multism software.

while L_1-L_{13} are derived using equation (1). The U-slot consists of three arms, equivalent to three series L-C branches, all connected in parallel. The H-slot consists of five branches, each consisting of series L-C branches. The circular slots consist of five capacitances created by the gaps; and four inductances created by the space between any two slots in the five circular slots. The parameter g used in the calculation is the width of each slot.

NI Multism software and the same 1V-peak AC voltage source are used for the circuit simulation. From Fig. 4, it can be observed that the output voltage, measured across the capacitor C_{15} is 8.25 nV, which is about 67% reduction compared to the reference antenna. It can be inferred that the decrease in voltage is a consequence of the additional U-slot, H-slot, and the five circular slots, which have collectively absorbed the coupling field emanating from the antenna. These etched structures are responsible for reducing the surface currents responsible for the mutual coupling between the two antennas when brought very close to each other. The presented equivalent circuits that demonstrate the output voltage reduction verify the concept of self-decoupling.

C. WIDE BAND AND SELF-ISOLATION MECHANISM

Herein, we explain the self-isolation technique employing the surface current distributions. In addition, we demonstrate how the different incorporated slots can simultaneously increase the matching bandwidth as well as increase the isolation in a MIMO array configuration.

It is well known that microstrip patch antennas are very effective because of their simple, robust, and compact structure. However, microstrip antennas are limited by low bandwidth, gain, and surface waves [4]. According to [34], the surface wave is predominant in a microstrip antenna if

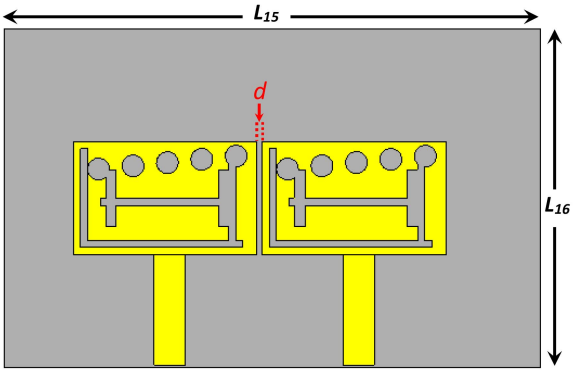

FIGURE 5. 1 × 2 MIMO antenna configuration of the self-isolated 5G mm-wave antenna ($d = 0.2$ mm).

the normalized substrate electrical thickness h/λ_0 satisfies the condition:

$$\frac{h}{\lambda_0} \geq \frac{0.3}{2\pi\sqrt{\epsilon_r}} \tag{4}$$

where h is the substrate thickness, λ_0 is the wavelength in free space, and ϵ_r is the dielectric constant of the substrate. Substituting the parameters of our antenna in (4), the left side and right side of the equation are approximately 0.06 and 0.03, respectively. Hence, it is evident that the surface waves effect is a potential cause for mutual coupling in this MIMO antenna. Apart from the surface waves, space waves (i.e., near-fields) also contribute to coupling in microstrip antennas, in the near-field region of the antenna, especially if the distance between the antenna elements is less than half wavelengths. This coupling effect is confined in the region above the substrate of the coupled patch antennas [35].

One way to improve the impedance bandwidth of the antenna is through the use of slots [36]. Slots enable more resonant modes to be excited in the patch by interrupting the uniformity of the patch, thereby, inducing perturbations, counteracting or constraining EM waves. This will disturb the surface current distribution in the patch, resulting in multiple resonances being excited in the patch. The EM wave propagation can be effectively controlled by meticulously optimizing the slots dimensions and locations, which can eventually alter the inductive and capacitive response of the entire patch. Slots' dimensions and locations were chosen by carefully observing the current paths on the surface of the antenna. The disturbed surface current introduced due to the slots is responsible for the increase in the isolation between the antenna elements when the positions and dimensions of the slots are carefully optimized. To ascertain the impedance bandwidth improvement and isolation enhancement capability of the slots, the antenna is arranged in a 1×2 configuration, as shown in Fig. 5 with dimension $L_{15} = 19$ mm X $L_{16} = 12$ m, and edge-to-edge separation of $d = 0.2$ mm, which is approximately $0.023\lambda_0$ at 35 GHz.

Fig. 6 shows the reflection and transmission coefficients of the reference antenna (Ref. A), Ref. B, Ref. C and the proposed antenna that are depicted in Fig. 1. It is clear

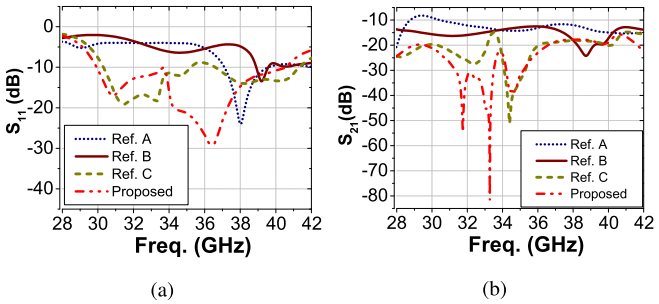

FIGURE 6. (a) S_{11} and (b) S_{21} throughout the antenna evolution from the reference 1 × 2 MIMO antenna (Ref. A) to the proposed 1 × 2 self-isolated MIMO antenna.

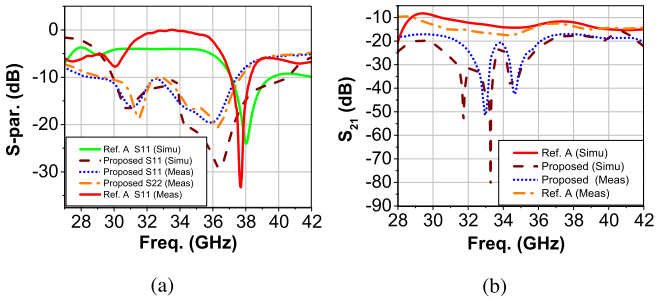

FIGURE 7. Measured and simulated (a) S_{11}-S_{22}, and (b) S_{21} of the reference 1 × 2 MIMO antenna (Ref. A) and the proposed 1 × 2 self-isolated MIMO antenna.

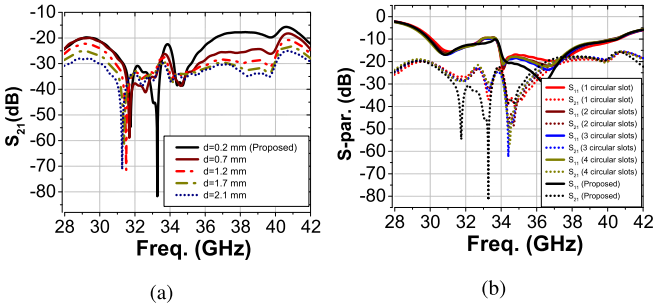

FIGURE 8. S-parameters of the proposed 1 × 2 self-isolated 5G mm-wave antenna with changing (a) the inter-element distance (*d*), and (b) the number of circular slots.

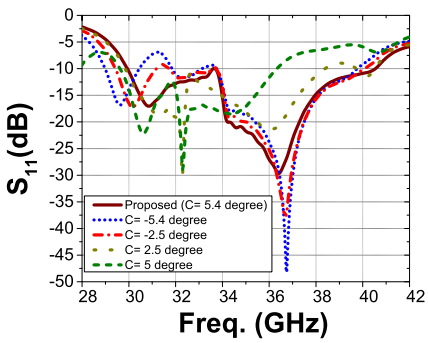

FIGURE 9. Effect of changing the tilt angle "c" of the circular slots on the reflection coefficient of the proposed 1 × 2 self-isolated 5G mm-wave antenna.

that the reference antenna (Ref. A) has a limited bandwidth between 37-40 GHz with a transmission coefficient of −11 dB at 38 GHz. By carefully introducing the U-slot on the patch at an appropriate distance (see Ref B in Fig. 1), the impedance bandwidth of the antenna is reduced with a resonance around 39 GHz as shown in Fig. 6a, while the isolation increases to about −22 dB as seen in Fig. 6b. To further increase the impedance bandwidth and mutual isolation, another H-slot is inserted at L_8 from the U-slot as shown in Ref. C of Fig. 1 and the antenna geometry of Fig. 2. The combination of U- and H-slot slots alters the mean current path of the antenna, which consequently disturbs the current distribution on the patch, thereby, generating more resonances and improving the isolation. Clearly, the results of Fig. 6 show that the working bandwidth of the Ref. C antenna has been significantly enhanced to include dual bands of 30-35 GHz and 36.5-42 GHz with maximum isolation of −50 dB.

To enable the antenna work over a wider bandwidth, five circular slots are meticulously optimized and incorporated into the patch (see proposed in Figs. 1d and 2). It is clear from Fig. 6 that the antenna now resonates from 30-41 GHz with a maximum isolation improvement of 67 dB at 33.2 GHz compared to the reference antenna (Ref. A). It is worthy of note that the major contributor to the coupling reduction and bandwidth enhancement is the carefully placed H-slot in addition to the U-slot and circular slots. Figure 7 shows good agreement between the simulated and measured S_{11}, S_{22}, and S_{21} of the reference 1 × 2 array (Ref. A) and the proposed 1 × 2 self-isolated antenna array.

D. PARAMETRIC ANALYSES

This subsection highlights the results obtained by a rigorous tuning of some key antenna parameters to improve its overall performance. The parameters and dimensions of the antenna in Figs. 2 and 5 are tuned and the results are discussed. Fig. 8a illustrates the effect of changing the edge-to-edge distance on the isolation characteristics while keeping other parameters constant. The isolation increases as the distance between the two antennas increases. However, the chosen smallest distance in this work ($d = 0.2$ *mm*) still exhibits very good isolation; less than 20 dB throughout the working bandwidth, fulfilling MIMO isolation requirements. The reflection coefficient is not affected by the change of the inter-element spacing, hence, not shown. Fig. 8b depicts the effect of the number of circular slots on the S-parameters while keeping other parameters constant. The proposed antenna with five slots exhibits the best reflection and transmission characteristics over the 30-41 GHz impedance bandwidth.

The effect of changing the tilting angle "c" of the five circular slots (see Fig. 2) on the reflection coefficient of the proposed 1 × 2 self-isolated MIMO antenna is shown in Fig. 9. The widest impedance bandwidth is observed when c = 5.4°.

Fig. 10a depicts that L_8 = 1.24 mm (see Fig. 2) is the best position to place the H-slot above the U-slot to obtain the desired reflection and transmission characteristics. Furthermore, Fig. 10b shows that the optimum rectangular slot width L_{14} to obtain the best reflection and

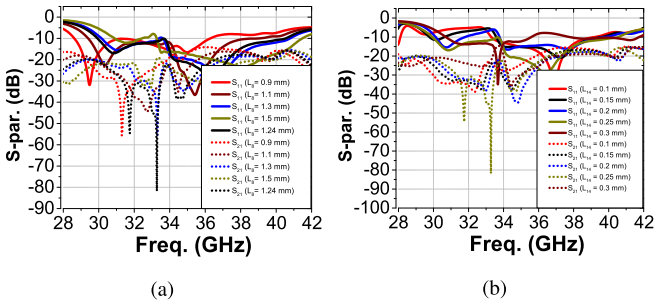

FIGURE 10. Effect of changing (a) L_8, and (b) rectangular slot width (L_{14}), on the S-parameters of the proposed self-isolated 1 × 2 5G mm-wave antenna.

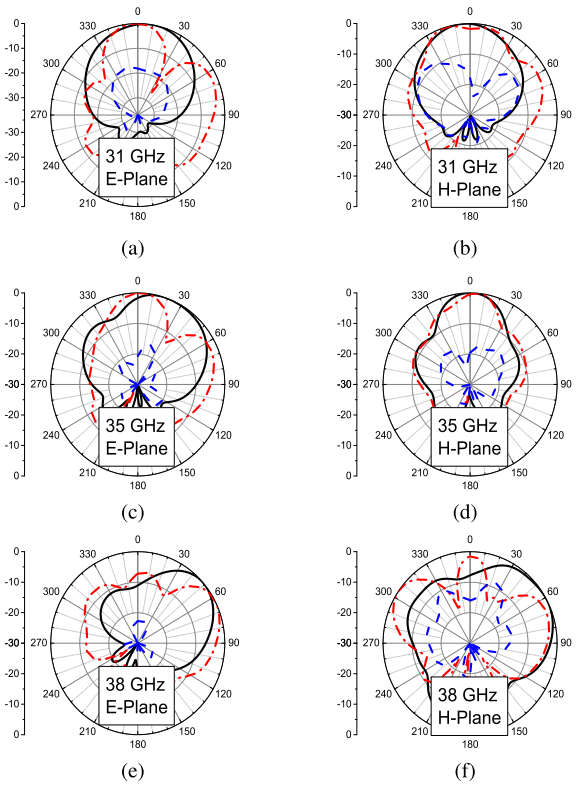

FIGURE 11. Simulated E-plane (left) and H-plane (right) radiation patterns of the proposed 1 × 2 MIMO antenna compared with the Ref. (A) MIMO antenna at 31, 35, and 38 GHz. [Black solid = Co-polar, proposed antenna. Red dashed = Co-polar, Ref. A antenna. Blue-dashed = Cross-polar, proposed antenna.].

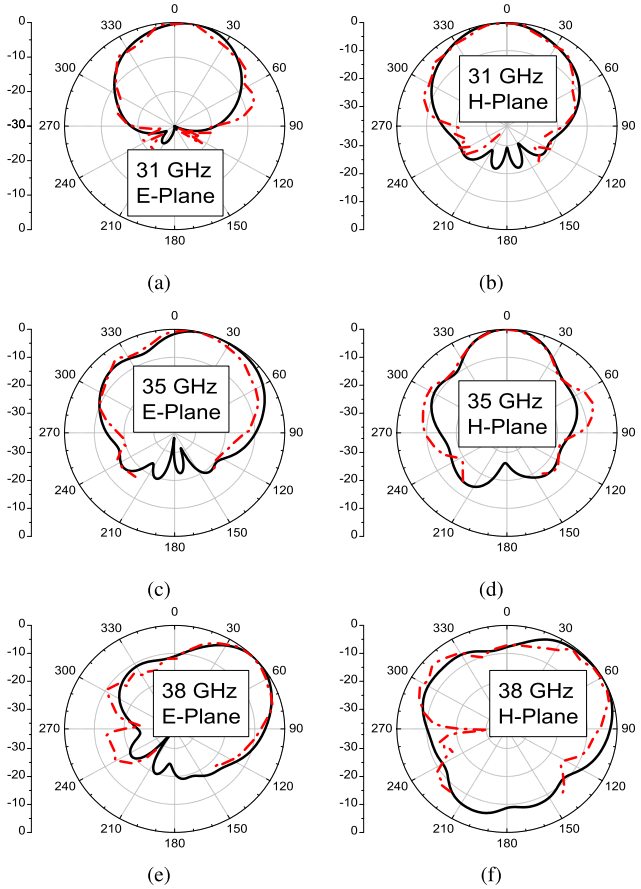

FIGURE 12. Measured (dashed) and simulated (solid) E-plane (left) and H-plane (right) radiation patterns of the proposed 1 × 2 MIMO antenna at 31, 35, and 38 GHz.

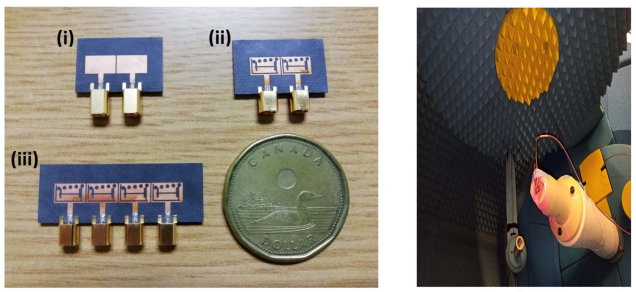

FIGURE 13. (a) Fabricated antennas: (i) Ref. A (ii) 1 × 2, (iii) 1 × 4 MIMO antennas, (b) Radiation pattern measurements set-up.

isolation characteristics is 0.25 mm, while other parameters are unaltered.

E. FAR-FIELD PROPERTIES

Fig. 11 plots the simulated radiation patterns of the proposed self-isolated 1 × 2 5G mm-wave antenna compared with the reference array (Ref. A) in the E- and H-planes at 31, 35, and 38 GHz. After inserting the slots and as a result of the surface current reduction, the radiation patterns of the array become more directive along the broadside direction over the frequency band of interest. Furthermore, a slight beam deflection is observed at 38 GHz, which is expected because of the high bandwidth of the antenna. A good agreement between the simulated and measured radiation patterns of the proposed self-isolated mm-wave 1 × 2 antenna at 31, 35, and 38 GHz is depicted in Fig. 12. Fig. 13a shows the fabricated prototypes of the Ref. A, 1 × 2, and 1 × 4 MIMO antennas. Fig. 13b shows the radiation pattern measurement set-up in an anechoic chamber.

III. MIMO ANTENNA CONFIGURATION

To verify the MIMO capability of the proposed antenna, a 4-element array is designed and arranged along the x-axis (H-plane) as shown in Fig. 14 with an edge-to-edge distance of $d = 0.2$ *mm*. The simulated surface current distribution

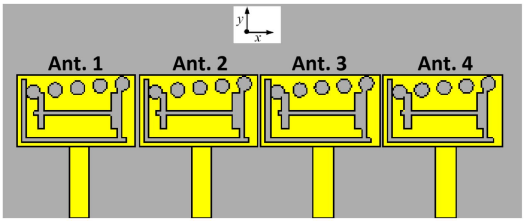

FIGURE 14. 1 × 4 MIMO configuration of the proposed self-isolated 5G mm-wave antenna.

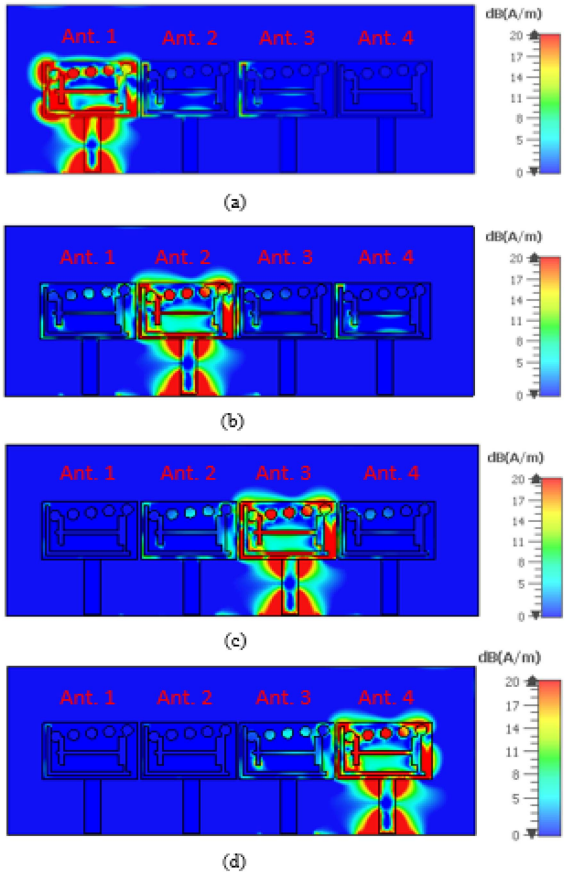

FIGURE 15. Surface current distribution of the 1 × 4 MIMO configuration of the proposed self-isolated 5G mm-wave antenna at 33 GHz when (a) Ant.1, (b) Ant. 2, (c) Ant. 3, and (d) Ant. 4 is excited.

of the 1×4 antenna when one port is excited, and the others are terminated with a matched load at 33 GHz is shown in Fig. 15. Fig. 15a shows that the surface current diminishes as the distance between the excited antenna (Ant.1) and the other antennas increases. Ant. 4 has almost no surface current when Ant. 1 is excited. Additionally, when Ant. 2 is excited, Ant. 1 and Ant. 3 exhibit nearly the same small surface current distribution, while Ant. 4 reveals a minimal surface current, as shown in Fig. 15b. The same phenomenon is observed when Ant. 3 or Ant. 4 are excited, as shown in Figs. 15c and 15d. This shows the effectiveness of the added slots in mitigating the surface currents.

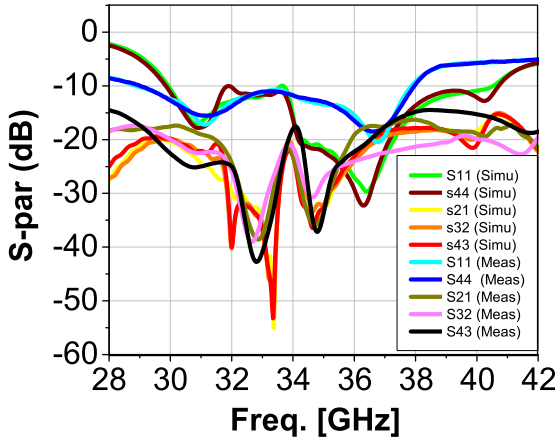

FIGURE 16. S-parameters of the 1 × 4 MIMO antenna configuration of the proposed self-isolated 5G mm-wave antenna.

The measured and simulated S-parameters of the 1×4 MIMO antenna are depicted in Fig. 16. The reflection coefficient of the antenna remains almost the same for all four elements, while the coupling effects are mostly below -20 dB throughout the desired impedance bandwidth of 30-41 GHz, demonstrating very good MIMO isolation properties.

The measured and simulated E- and H-plane radiation patterns of the 1×4 MIMO array at 32 GHz are depicted in Fig. 17. The MIMO array exhibits consistent broadside radiation characteristics in both planes with almost no beam deflection.

The gain and efficiency are two important performance indices of an antenna that relates the radiated power to the input power. Coupling affects the effective input impedance of the elements (see Fig. 6a), resulting in a higher reflection than isolated elements, and thus, reduces the radiated power. Therefore, reducing the coupling effect on the element matching enhances the radiated power improving the gain and efficiency [5], [6], [7]. Moreover, considerable amount of power is coupled to the neighbouring antennas in case of poor isolation between the MIMO elements.

Fig. 18a depicts that the 1×2 antenna array peak gain has been improved compared to the reference antenna (Ref. A) without slots, owing to the isolation improvement over the working bandwidth. It is worth noting that the proposed MIMO antenna has good gain flatness except for the notched band at 34 GHz. This is due to the low isolation improvement observed around 34 GHz, as seen in Fig. 7b.

However, Fig. 18(a-b) shows that the gain and total efficiency at 34 GHz of 7.5 dB and 90%, are still sufficient for efficient radiation. The simulated total efficiency of the 1×2 antenna array is shown in Fig. 18b. As expected, the total efficiency has an average value of about 91% compared with 55% of the reference antenna (Ref. A). The efficiency increase is mainly due to the isolation enhancement of the antenna.

The Envelope correlation coefficient (ECC) is an important performance criterion in MIMO antennas. It can be

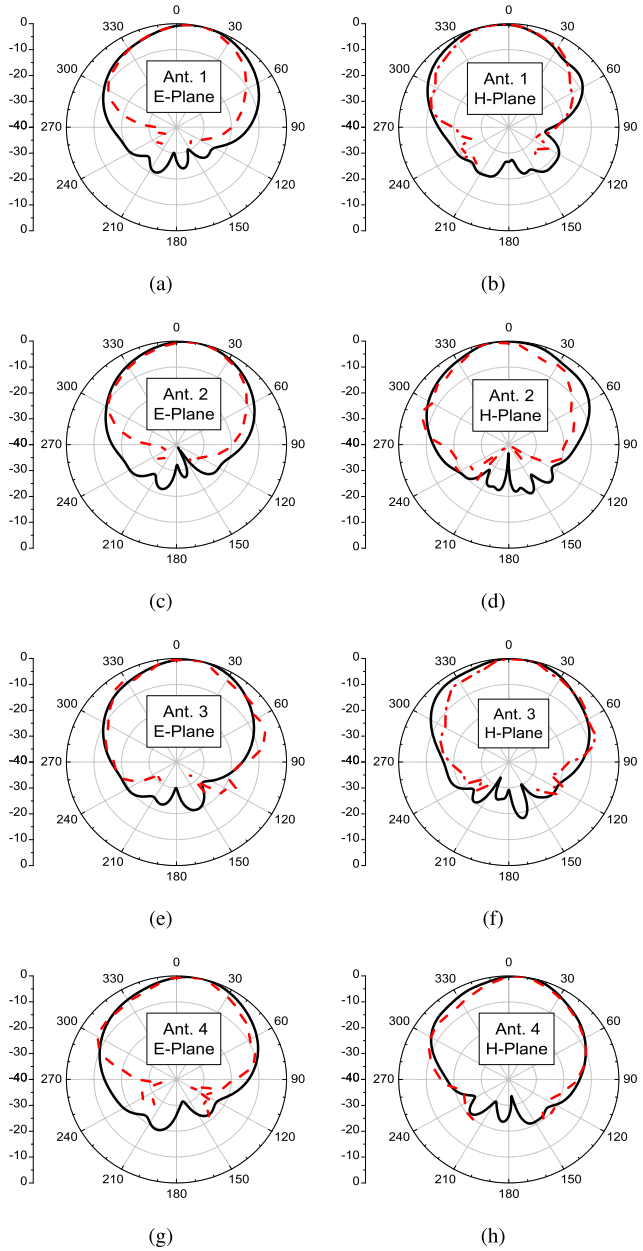

FIGURE 17. Measured (dashed) and simulated (solid) E-plane (left) and H-plane (right) radiation patterns of the 1 × 4 MIMO configuration of the proposed self-isolated antenna at 32 GHz of Ant. 1, Ant. 2, Ant. 3, and Ant. 4, respectively, from top to bottom.

determined using S-parameters or far-field characteristics. The S-parameters method is useful when efficiency is considerably high (i.e., lossless antenna) [37]. The far-fields method is more reliable for lossy antennas as it considers the far-fields characteristics of the two antennas. ECC based on far-fields can be expressed as [37]:

$$ECC = \frac{|\iint_{4\pi}[F_1(\theta,\phi) * F_2(\theta,\phi)]d\Omega|^2}{\iint_{4\pi}|F_1(\theta,\phi)|^2 d\Omega \iint_{4\pi}|F_2(\theta,\phi)|^2 d\Omega} \quad (5)$$

where $F_1(\theta,\phi)$ is the field pattern when antenna 1 is excited and antenna 2 is terminated by 50 Ω load, and vice-versa for $F_2(\theta,\phi)$. The simulated ECC of the reference (Ref. A) and

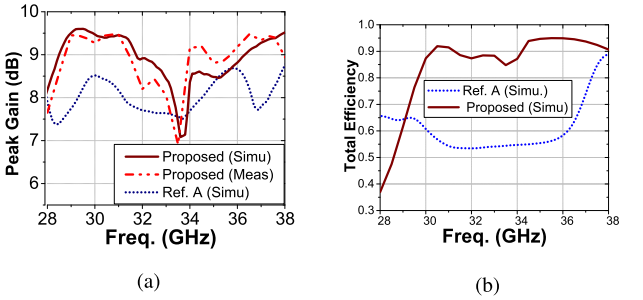

FIGURE 18. (a) Peak gain, and (b) Total efficiency of the proposed 1 × 2 MIMO antenna compared to the reference antenna (Ref. A).

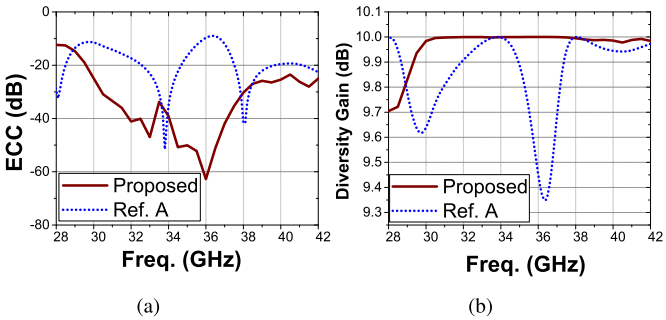

FIGURE 19. (a) Envelope correlation coefficient (ECC) based on far-fields, and (b) Diversity gain of the proposed 1 × 2 MIMO antenna compared to the reference antenna (Ref. A).

the proposed 1×2 MIMO antennas, based on far field parameters, is depicted in Fig. 19a. The proposed antenna exhibits ECC less than −20 dB over the impedance bandwidth, with a considerable coupling reduction compared with the reference antenna (Ref. A) indicating an isolation improvement.

The diversity gain is another important parameter for the evaluation of the MIMO system and can be obtained using [39]:

$$Diversity\ gain = 10\sqrt{1 - |\,ECC\,|} \quad (6)$$

where 10 is the apparent maximum diversity gain. The ECC of the proposed antenna is less than 0.01, thereby, making its diversity gain around 10 dB within the operational bandwidth as depicted in Fig. 19b. This improved diversity gain is a result of the improved isolation between the MIMO elements. Another important performance index for MIMO antenna is the Total Active Reflection Coefficient (TARC). As stated in [40], TARC is defined as the ratio of the square-root of total reflected power divided by the square-root of total incident power. Unlike the traditional S_{11} of a single antenna, TARC considers the effect of the mutual coupling between the MIMO elements and the incident wave phase. For a two-element MIMO antenna, TARC can be calculated as [40]

$$TARC = \sqrt{\left(\left|\left(s_{11} + s_{12}e^{j\theta}\right)\right|^2 + \left|\left(s_{21} + s_{22}e^{j\theta}\right)\right|^2\right)}/\sqrt{2} \quad (7)$$

Fig. 20 shows the TARC of the proposed 1×2 self-isolated MIMO antenna in the presence of mutual coupling. It can

TABLE 2. Performance of the proposed mm-wave antenna compared to recent literature.

Year/Ref.	Type of Antenna	Edge-to-edge spacing	Method of decoupling	Impedance bandwidth (%)	Peak Efficiency (%)	Peak Gain (dB)	Maximum isolation improvement
2018 [8]	printed patch	0.67λ	CSRR	24.5-25.5 GHz (4%)	-	-	31.8 dB
2019 [21]	printed patch	$0.016\lambda_0$	near-field resonator	2.1-2.3 GHz (6.1%)	80	5.1	20 dB
2021 [22]	printed patch	$0.027\lambda_0$	dielectric block	4.32-5.48 GHz (23.6%)	97	7.4	20 dB
2019 [25]	printed patch	$0.014\lambda_0$	self-isolation	3.4-3.6 GHz (5.7%)	58	-	17 dB
2020 [31]	printed patch	$0.5\lambda_0$	self-isolation	3.4-3.6 GHz (5.7%)	-	7.5	37 dB
2020 [38]	printed patch	$0.1\lambda_0$	EBG, CSRR and DGS	3.1-3.4 GHz (9.2%)	-	4.9	12 dB
Proposed	printed patch	$0.023\lambda_0$	self-isolation	28-37.5 GHz (29%)	96	9.6	35 dB

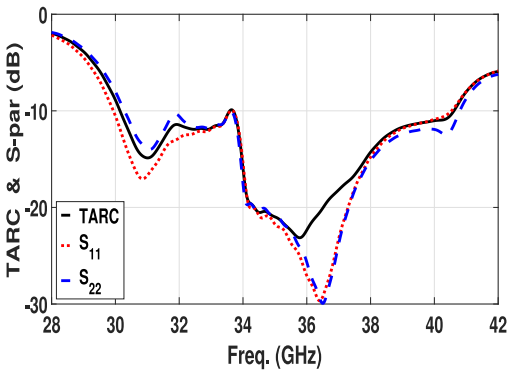

FIGURE 20. Total Active Reflection Coefficient (TARC) of the proposed 1 × 2 self-isolated MIMO antenna compared to traditional reflection coefficients (S_{11} and S_{22}) of the same antenna.

be observed that TARC exhibits similar behaviour as the antenna's traditional reflection coefficients (S_{11} and S_{22}). However, the 10-dB TARC bandwidth is slightly affected due to the mutual coupling effect.

Table 2 depicts the comparison of the proposed antenna with recent literature. The proposed antenna exhibits the largest impedance bandwidth *combined* with high efficiency, gain, and maximum isolation improvement with minimal edge-to-edge spacing. The proposed antenna is the only design in Table 2 that simultaneously acquires all these attractive features without compromising any fundamental design objective.

ACKNOWLEDGMENT

The authors acknowledge Mr Sagiru Gaya from Khalifa University for the valuable discussions during this work.

IV. CONCLUSION

A novel, simple, and low-cost self-isolated mm-wave 1×2 MIMO antenna with an impedance bandwidth of 28-37.5 GHz, 51 dB maximum isolation, and edge-to-edge spacing of $0.023\lambda_0$ has been presented. No additional or external isolating structures have been used. Various antenna parameters have been investigated to achieve high bandwidth and the smallest possible edge-to-edge spacing. Moreover, a 1×4 MIMO configuration of the antenna has been presented and analyzed. Good agreement between the measured and simulated results has been achieved. Compared to previously published designs, the proposed MIMO antenna exhibits a wide bandwidth greater than 29%, improved efficiency greater than 90%, minimal envelope correlation coefficient less than 0.005, and significant isolation improvement greater than 50 dB with minimal inter-element spacing.

REFERENCES

[1] J. G. Andrews et al., "What will 5G be?" *IEEE J. Sel. Areas Commun.*, vol. 32, no. 6, pp. 1065–1082, Jun. 2014.
[2] W. Hong, "Solving the 5G mobile antenna puzzle: Assessing future directions for the 5G mobile antenna paradigm shift," *IEEE Microw. Mag.*, vol. 18, no. 7, pp. 86–102, Nov./Dec. 2017.
[3] X. Shen, Y. Liu, L. Zhao, G. Huang, X. Shi, and Q. Huang, "A miniaturized microstrip antenna array at 5G millimeter-wave band," *IEEE Antennas Wireless Propag. Lett.*, vol. 18, no. 8, pp. 1671–1675, Aug. 2019.
[4] S. F. Jilani and A. Alomainy, "Millimetre-wave T-shaped MIMO antenna with defected ground structures for 5G cellular networks," *IET Microw. Antennas Propagat.*, vol. 12, no. 5, pp. 672–677, 2018.
[5] J. Qiang, F. Xu, and W. Fan, "Reducing mutual coupling of Millimeter wave array antennas by fractal defected ground structure," in *Proc. 12th Int. Symp. Antennas Propagat. EM Theory (ISAPE)*, Dec. 2018, pp. 1–3.
[6] S. Gupta, Z. Briqech, A. R. Sebak, and T. Ahmed Denidni, "Mutual-coupling reduction using metasurface corrugations for 28 GHz MIMO applications," *IEEE Antennas Wireless Propag. Lett.*, vol. 16, pp. 2763–2766, 2017.
[7] A. Dadgarpour, B. Zarghooni, B. S. Virdee, T. A. Denidni, and A. A. Kishk, "Mutual coupling reduction in dielectric resonator antennas using Metasurface shield for 60-GHz MIMO systems," *IEEE Antennas Wireless Propag. Lett.*, vol. 16, pp. 477–480, 2017.
[8] R. Selvaraju, M. H. Jamaluddin, M. R. Kamarudin, J. Nasir, and M. H. Dahri, "Mutual coupling reduction and pattern error correction in a 5G Beamforming linear array using CSRR," *IEEE Access*, vol. 6, pp. 65922–65934, 2018.
[9] S. I. Naqvi et al., "An integrated antenna system for 4G and Millimeter-wave 5G future Handheld devices," *IEEE Access*, vol. 7, pp. 116555–116566, 2019.
[10] R. Karimian, A. Kesavan, M. Nedil, and T. A. Denidni, "Low-mutual-coupling 60-GHz MIMO antenna system with frequency selective surface wall," *IEEE Antennas Wireless Propag. Lett.*, vol. 16, pp. 373–376, 2017.
[11] M. Al-Hasan, I. B. Mabrouk, E. R. F. Almajali, M. Nedil, and T. A. Denidni, "Hybrid isolator for mutual-coupling reduction in Millimeter-wave MIMO antenna systems," *IEEE Access*, vol. 7, pp. 58466–58474, 2019.
[12] Y. M. Pan, X. Qin, Y. X. Sun, and S. Y. Zheng, "A simple decoupling method for 5G Millimeter-wave MIMO dielectric resonator antennas," *IEEE Trans. Antennas Propag.*, vol. 67, no. 4, pp. 2224–2234, Apr. 2019.

[13] Y. Zhang, J. Deng, M. Li, D. Sun, and L. Guo, "A MIMO dielectric resonator antenna with improved isolation for 5G mm-wave applications," *IEEE Antennas Wireless Propag. Lett.*, vol. 18, no. 4, pp. 747–751, Apr. 2019.

[14] S. Gaya, O. Sokunbi, A. Hamza, S. I. M. Sheikh, and H. Attia, "Multiple-input-multiple-output antenna with pattern reconfiguration and correlation reduction for wlan applications," *Eng. Rep.*, vol. 2, no. 12, 2020, Art. no. e12272.

[15] S. Zhu, H. Liu, Z. Chen, and P. Wen, "A compact gain-enhanced Vivaldi antenna array with suppressed mutual coupling for 5G mmWave application," *IEEE Antennas Wireless Propag. Lett.*, vol. 17, no. 5, pp. 776–779, May 2018.

[16] T. H. Jang, H. Y. Kim, D. M. Kang, S. H. Kim, and C. S. Park, "60 GHz low-profile, wideband dual-polarized U-slot coupled patch antenna with high isolation," *IEEE Trans. Antennas Propag.*, vol. 67, no. 7, pp. 4453–4462, Jul. 2019.

[17] M. J. Al-Hasan, T. A. Denidni, and A. R. Sebak, "Millimeter-wave compact EBG structure for mutual coupling reduction applications," *IEEE Trans. Antennas Propag.*, vol. 63, no. 2, pp. 823–828, Feb. 2015.

[18] O. Sokunbi and H. Attia, "Highly reduced mutual coupling between wideband patch antenna array using multiresonance EBG structure and defective ground surface," *Microw. Opt. Technol. Lett.*, vol. 62, no. 4, pp. 1628–1637, 2020.

[19] O. Sokunbi, H. Attia, and S. I. Sheikh, "Microstrip antenna array with reduced mutual coupling using slotted-ring EBG structure for 5G applications," in *Proc. IEEE Int. Symp. Antennas Propagat. USNC-URSI Radio Sci. Meeting*, Jul. 2019, pp. 1185–1186.

[20] D. Gao, Z.-X. Cao, S. D. Fu, X. Quan, and P. Chen, "A novel slot-array defected ground structure for decoupling microstrip antenna array," *IEEE Trans. Antennas Propag.*, vol. 68, no. 10, pp. 7027–7038, Oct. 2020.

[21] M. Li, B. G. Zhong, and S. W. Cheung, "Isolation enhancement for MIMO patch antennas using near-field resonators as coupling-mode transducers," *IEEE Trans. Antennas Propag.*, vol. 67, no. 2, pp. 755–764, Feb. 2019.

[22] M. Li, M. Y. Jamal, L. Jiang, and K. L. Yeung, "Isolation enhancement for MIMO patch antennas sharing a common thick substrate: Using a dielectric block to control space-wave coupling to cancel surface-wave coupling," *IEEE Trans. Antennas Propag.*, vol. 69, no. 4, pp. 1853–1863, Apr. 2021.

[23] B.-J. Niu and J. Tan, "Compact self-isolated MIMO antenna system based on quarter-mode SIW cavity," *Electron. Lett.*, vol. 55, no. 10, pp. 574–576, 2019.

[24] Y. Li, C.-Y.-D. Sim, Y. Luo, and G. Yang, "High-isolation 3.5 GHz eight-antenna MIMO array using balanced open-slot antenna element for 5G Smartphones," *IEEE Trans. Antennas Propag.*, vol. 67, no. 6, pp. 3820–3830, Jun. 2019.

[25] Z. Ren, A. Zhao, and S. Wu, "MIMO antenna with compact decoupled antenna pairs for 5G mobile terminals," *IEEE Antennas Wireless Propag. Lett.*, vol. 18, no. 7, pp. 1367–1371, Jul. 2019.

[26] A. Zhao and Z. Ren, "Multiple-input and multiple-output antenna system with self-isolated antenna element for fifth-generation mobile terminals," *Microw. Opt. Technol. Lett.*, vol. 61, no. 1, pp. 20–27, 2019.

[27] J. Sui and K.-L. Wu, "Self-curing decoupling technique for two inverted-F antennas with capacitive loads," *IEEE Trans. Antennas Propag.*, vol. 66, no. 3, pp. 1093–1101, Mar. 2018.

[28] K.-L. Wong, C.-C. Wan, and L.-Y. Chen, "Self-decoupled compact metal-frame LTE MIMO antennas for the smartphone," *Microw. Opt. Technol. Lett.*, vol. 60, no. 5, pp. 1170–1179, 2018.

[29] L. Sun, Y. Li, Z. Zhang, and H. Wang, "Self-decoupled MIMO antenna pair with shared radiator for 5G Smartphones," *IEEE Trans. Antennas Propag.*, vol. 68, no. 5, pp. 3423–3432, May 2020.

[30] A. Zhao and Z. Ren, "Size reduction of self-isolated MIMO antenna system for 5G mobile phone applications," *IEEE Antennas Wireless Propag. Lett.*, vol. 18, no. 1, pp. 152–156, Jan. 2019.

[31] H. Lin, Q. Chen, Y. Ji, X. Yang, J. Wang, and L. Ge, "Weak-field-based self-decoupling patch antennas," *IEEE Trans. Antennas Propag.*, vol. 68, no. 6, pp. 4208–4217, Jun. 2020.

[32] D. M. Pozar, *Microwave Engineering*, 4th ed. Hoboken, NJ, USA: Wiley, 2011. [Online]. Available: https://cds.cern.ch/record/882338

[33] Y.-K. Yoon, M. Allen, and A. Hunt, "Tunable ferroelectric capacitor with low-loss electrodes fabricated using reverse side exposure," in *Proc. 53rd Electron. Compon. Technol. Conf.*, 2003, pp. 1534–1540.

[34] M. M. Nikolic, A. R. Djordjevic, and A. Nehorai, "Microstrip antennas with suppressed radiation in horizontal directions and reduced coupling," *IEEE Trans. Antennas Propag.*, vol. 53, no. 11, pp. 3469–3476, Nov. 2005.

[35] Z. Qamar, U. Naeem, S. A. Khan, M. Chongcheawchamnan, and M. F. Shafique, "Mutual coupling reduction for high-performance densely packed patch antenna arrays on finite substrate," *IEEE Trans. Antennas Propag.*, vol. 64, no. 5, pp. 1653–1660, May 2016.

[36] S. T. Fan, Y. Z. Yin, B. Lee, W. Hu, and X. Yang, "Bandwidth enhancement of a printed slot antenna with a pair of parasitic patches," *IEEE Antennas Wireless Propag. Lett.*, vol. 11, pp. 1230–1233, 2012.

[37] M. S. Sharawi, "Current misuses and future prospects for printed multiple-input, multiple-output antenna systems [wireless corner]," *IEEE Antennas Propag. Mag.*, vol. 59, no. 2, pp. 162–170, Apr. 2017.

[38] Z. Yang, J. Xiao, and Q. Ye, "Enhancing MIMO antenna isolation characteristic by manipulating the propagation of surface wave," *IEEE Access*, vol. 8, pp. 115572–115581, 2020.

[39] J. Park, M. Rahman, and H. N. Chen, "Isolation enhancement of wideband MIMO array antennas utilizing resistive loading," *IEEE Access*, vol. 7, pp. 81020–81026, 2019.

[40] S. H. Chae, S.-K. Oh, and S.-O. Park, "Analysis of mutual coupling, correlations, and TARC in WiBro MIMO array antenna," *IEEE Antennas Wireless Propag. Lett.*, vol. 6, pp. 122–125, 2007.